*J. M. Bloom**

Appendix J – the Deformation Plasticity Failure Assessment Diagram (DPFAD) Approach to Evaluation of Flaws in Ferritic Piping

REFERENCE Bloom, J. M., **Appendix J – the deformation plasticity failure assessment diagram (DPFAD) approach to evaluation of flaws in ferritic piping**, *Defect Assessment in Components – Fundamentals and Applications*, ESIS/EGF9 (Edited by J. G. Blauel and K.-H. Schwalbe) 1991, Mechanical Engineering Publications, London, pp. 1073–1094.

ABSTRACT This paper discusses an ASME Code procedure currently under consideration by the ASME Section XI Working Group on Flaw Evaluation. The procedure was initially put forth in 1985 for evaluating the acceptability of flaws detected in piping during in-service inspection for certain materials, identified in Article IWB-3640 of the ASME Boiler and Pressure Vessel Code Section XI 'Rules for In-service Inspection of Nuclear Power Plant Components,' for which the fracture toughness is not high enough to justify acceptance based solely on the plastic limit load evaluation methodology of Appendix C and IWB-3641. The procedure, referred to as Appendix J, originally included two approaches: a J integral-based tearing instability (J–T) analysis and the deformation plasticity failure assessment diagram (DPFAD) methodology. During the last few years, the DPFAD part of Appendix J was developed into code format and with the support of the members of the ASME Section XI Working Group on Flaw Evaluation and the Electric Power Research Institute, Appendix J has been shown to be a valid approach for the assessment of both circumferential and axial part-through wall flaws in ferritic piping.

In Appendix J, a general DPFAD approach was simplified for application to part-through wall flaws in ferritic piping through the use of a single DPFAD curve for circumferential flaws. Axial flaws are handled using two DPFAD curves where the ratio of flaw depth to wall thickness is used to determine the appropriate DPFAD curve. Flaws are evaluated in Appendix J by comparing the actual pipe applied stress with the allowable stress with the appropriate safety factors for the flaw size at the end of the evaluation period. Assessment points for circumferential and axial flaws are plotted on the appropriate failure assessment diagram. If the assessment points with the specified safety factors fall inside the appropriate failure assessment diagram curve, the inspection flaw is allowable. If the assessment points fall outside the diagram curve, the pipe must be repaired or replaced. Finally, this paper summarises the experimental test predictions of the results of the Battelle Columbus Laboratory experiments, the Eiber experiments, and the JAERI tests using the Appendix J DPFAD methodology.

Notation

a	General depth dimension for a flaw (inches)
a_f	Maximum depth to which the detected flaw is calculated to grow by the end of the evaluation period (inches)
E'	$E/(1-\nu^2)$ (ksi)
E	Young's modulus (ksi)
σ_{ys}	Yield strength (ksi)
J_{IC}	Measure of toughness due to crack extension at upper shelf, transition, and lower shelf temperatures (in-lbs/in^2)

* Structural Mechanics Section, Babcock and Wilcox, A McDermott Company, Research and Development Division Alliance, Ohio 44601, USA.

l	Flaw length of an axial through-the-wall flaw (inches)
l_{crit}	Critical flaw length for stability of an axial through-the-wall flaw (inches)
σ_h	Maximum applied pipe hoop stress (ksi)
t	Pipe wall thickness (inches)
P_m	Primary membrane stress in the pipe at the flaw (ksi)
P_b	Primary bending stress in the pipe at the flaw (ksi)
P'_b	Bending stress at limit load for any combination of primary and expansion stress (ksi)
θ	One-half of the final flaw angle (see Fig. 3) (radians)
ν	Poisson's ratio
β	Angle to neutral axis of flawed pipe (radians)
(SF)	Safety factor (dimensionless)
K_I	Mode I stress intensity factor (ksi $\sqrt{\text{in}}$)
P_e	Pipe expansion stress (ksi)
F_m	Parameter for circumferential flaw membrane stress intensity factor
F_b	Parameter for circumferential flaw bending stress intensity factor
p	Internal pressure (ksi)
R	Mean radius of pipe (inches)
R_1	Inside radius of pipe (inches)
R_2	Outside radius of pipe (inches)
Q	Flaw shape parameter (dimensionless)
σ_0, ε_0	Reference stress and strain as used in the Ramberg-Osgood equation (ksi, dimensionless)
G	Total elastic energy available per unit increase in crack surface area (in-lb/in^2)
$J_{applied}$	J-integral structural response (in-lb/in^2)
J_p	Plastic component of $J_{applied}$ (in-lb/in^2)
α, n	Ramberg-Osgood parameters (dimensionless)
CL	Orientation of a test specimen in the circumferential direction with longitudinal crack plane orientation
$J_R(\Delta a)$	Material's J integral resistance to ductile tearing at a prescribed Δa value obtained from accepted test procedures (in-lbs/in^2)
Δa	Amount of ductile flaw extension (inches)
P'_m	Membrane stress at reference limit load for any combination of primary and expansion stresses (ksi)
K'_r	Brittle fracture component of the assessment point defined by the ratio of the stress intensity factor to the material fracture toughness (dimensionless)
K_r	Ordinate of the FAD curve (dimensionless)
S'_r	Limit load component of the assessment point defined for circumferential flaws by the ratio of the applied stress to the stress at reference limit load (P'_m) and for axial flaws as the ratio of pressure to the reference limit (load) pressure (P_0) (dimensionless)
S_r	Abscissa of the FAD curve (dimensionless)
σ_f	The material's flow stress, equal to the average of the yield stress (σ_{ys}) and the engineering ultimate stress (σ_{uts}) (ksi)
σ_{uts}	Engineering ultimate stress (ksi)
S_r^{cutoff}	Maximum value of S_r at the vertical (limit load) boundary of the failure assessment diagram curve (dimensionless)
J_I^e	Elastic J integral (in-lbs/in^2)
a'	Sum of the flaw depth plus the amount of ductile flaw crack extension (inches)
P_0	Reference limit (load) pressure (ksi)
$P_{ultimate}$	Limit load based on ultimate strength (Kips)
Γ_m	Factor in the reference limit load expression for P'_m reflecting the effect of flaw size (dimensionless)
γ	Factor in the reference limit load expression for P'_m reflecting the ratio of P_b to P_m (dimensionless)
R_c	Sum of the flaw depth and the inside radius of pipe (inches)
a^*	Equivalent flaw depth for a part through axial flaw in a pipe under internal pressure (inches)
F_1	Total geometry correction factor for an interior axial part through wall flaw in a pressurised pipe (dimensionless)
M'_1, M'_2, M'_3	Geometry correction factor for an interior axial part-through-wall flaw in a pressurised pipe which accounts for the flaw aspect ratio, a/l (dimensionless)
f_c	Geometry correction term that accounts for the flaw depth relative to the pipe size (dimensionless)

Introduction and background

Section XI of the ASME Code **(1)** and 10 CFR50 of the United States Code of Federal Regulations **(2)** require periodic inspection of reactor coolant pressure boundary components in operating commercial nuclear power plants. If flaws are found during inspection, evaluation using the acceptance standards of IWB-3500 in Section XI is required. Flaws larger than those specified in IWB-3500 can be evaluated further using the analysis procedures and acceptance criteria in IWB-3600.

Prior to 1983, evaluation procedures existed for only ferritic steel components four inches or greater in thickness. In the 1983 Winter Addenda to the ASME Code, procedures based on plastic collapse (limit load) for Class 1 austenitic steel piping were added. In 1985, revised evaluation procedures were incorporated in the Winter Addenda to the Code to allow consideration of certain low toughness welds where the possibility exists of failure mechanisms due to unstable flaw extension at loads lower than the plastic collapse loads.

These revised computational procedures in the 1985 Addenda were based on elastic–plastic fracture mechanics methodology using conservative approximate correction factors applied to the limit load expressions. This evaluation methodology appeared in Appendix C and IWB-3641 of the 1985 Addenda.

In 1983, the Working Group on Flaw Evaluation of Section XI began developing flaw evaluation procedures for ASME Class 1 ferritic piping. Flawed ferritic piping was recognised to have possible failure mechanisms which, depending on operating temperature could range from linear elastic (brittle) fracture to elastic–plastic ductile tearing to plastic collapse. This wide variation of failure mechanisms necessitated an evaluation procedure that could account for all these possible failure modes. The ASME Section XI Working Group on Flaw Evaluation approached this problem through the development of two separate appendixes to the Code; Appendix Z **(3)** and Appendix J.

Appendix Z first appeared in the 1988 Winter Addenda as Code Case N-463 in answer to the inquiry: 'Under Section XI, Division 1, may Class 1 ferritic piping containing a flaw that exceeds the acceptance standards of IWB-3514.2 be evaluated and accepted for continued service as provided in IWB-3132.4?' Appendix Z consists of a simple, step-by-step screening criterion based on the deformation plasticity failure assessment diagram (DPFAD) approach **(4)** to identify the relevant failure mechanisms and appropriate analysis methods. Separate analysis procedures are provided for brittle fracture, ductile tearing, and plastic collapse. For ductile tearing, correction factors similar to those of Appendix C are used based on elastic–plastic J integral solutions for through-wall flawed geometries using bounding stresses and lower bound material properties.

Appendix J developed in parallel with Appendix Z provides an alternate methodology using the DPFAD procedure **(5)** directly to determine acceptance of ferritic piping containing a flaw that exceeds the acceptance standards of IWB-3514.2. Flaws are evaluated in Appendix J by comparing the actual pipe applied stress with the allowable stress with the appropriate safety factors for the flaw size at the end of the evaluation period. Assessment points accounting for the actual pipe material properties through the input of the J_R resistance curve due to ductile flaw extension for circumferential and axial flaws are plotted on the appropriate failure assessment diagram. If the assessment points with the specified safety factors fall inside the appropriate failure assessment curve, the inspection flaw is allowable. If the assessment points fall outside the diagram curve, the pipe must be repaired or replaced.

This paper will first address an overview of the Appendix J procedure followed by a detailed discussion of the procedure. Details of the simplification of the general DPFAD methodology for part-through wall flaws for ferritic piping used in Appendix J will be presented, and lastly, validation of the simplified approach through comparisons with actual experimental test results of degraded nuclear piping will be discussed.

Appendix J procedure overview

The following is a summary of the analytical procedure.

(1) Determine the actual flaw configuration from the measured flaw in accordance with IWA-3000 of Section XI.
(2) Resolve the actual flaw into circumferential and axial flaw components.
(3) Determine the stresses normal to the flaw at the location of the detected flaw for normal operating (including upset and test) conditions and emergency and faulted conditions.
(4) Perform a flaw growth analysis to establish the end of evaluation period flaw dimensions, a_f and l_f.
(5) Obtain pipe material properties, E, σ_{ys}, σ_{uts}, and J_R or J_{IC}, at the temperatures required for analysis.
(6) Select the appropriate failure assessment diagram curve from Figs 1 and 2 according to flaw configuration, circumferential or axial, and for axial flaws according to the ratio of flaw depth to wall thickness (Fig. 3).
(7) Calculate the vertical cutoff, S_r^{cutoff}, for the selected failure assessment diagram curve.
(8) Calculate the assessment point coordinates (S_r', K_r') for the piping stresses P_m, P_b and P_e for circumferential flaws or p (pressure) for axial flaws using the specified safety factors in Table 1.

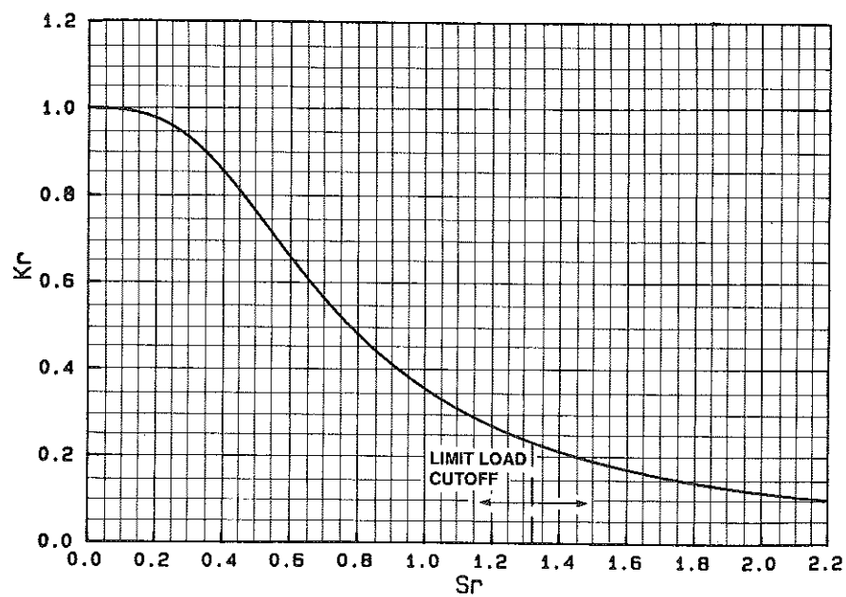

Fig 1 Failure assessment diagram curve for part-through-wall circumferential flaws

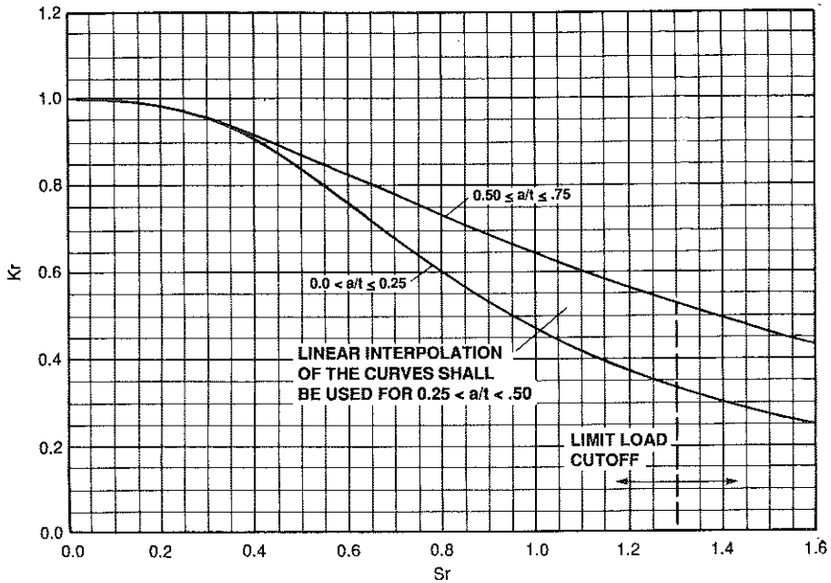

Fig 2 Failure assessment diagram curves for part-through-wall axial flaws

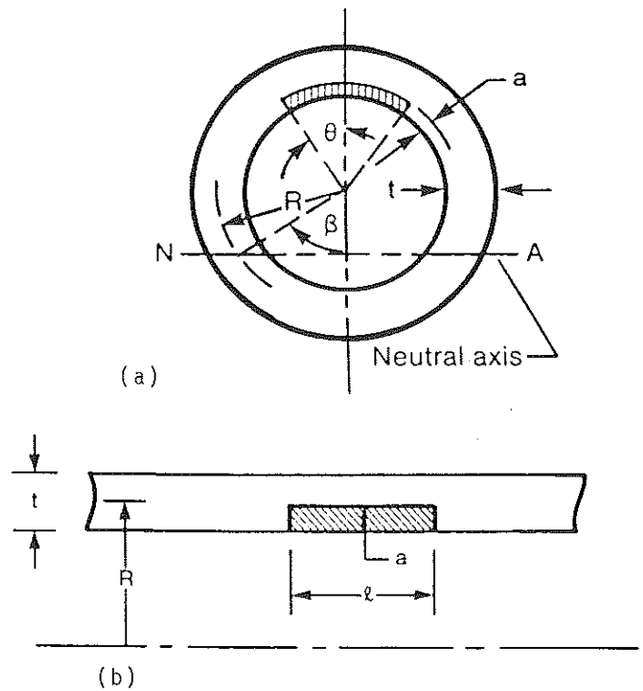

Fig 3 Flaw configurations for (a) a circumferential flaw and (b) an axial flaw

Table 1 Specified Safety Factors (SF)

Circumferential flaws	
Normal and upset conditions	2.77
Emergency and faulted conditions	1.39
Axial flaws	
Normal and upset conditions	3.0
Emergency and faulted conditions	1.5

(9) Plot the assessment point(s) calculated in procedure no. 8 on the appropriate failure assessment diagram and determine the acceptability of the pipe for continued service.

Detailed failure assessment diagram analysis

This section describes the detailed failure assessment diagram procedure for the evaluation of flaws in ferritic piping. The procedure involves:

- choosing the failure assessment diagram curve;
- calculating the failure assessment point coordinates;
- evaluating flaw acceptance determination.

Failure assessment diagram curves for ferritic piping are proposed for the following two flaw configurations:

- part-through-wall circumferential flaws under any combination of primary membrane, primary bending, and expansion stresses;
- axial flaws in pipes under internal pressure.

Figure 1 shall be used for part-through-wall circumferential flaws of depths up to 75 percent of the pipe wall thickness and lengths up to half the inside circumference of the pipe.

Figure 2 shall be used for axial flaws of depths up to 75 percent of the pipe wall thickness and lengths up to l_{crit}, where l_{crit} is given by the limit load condition for through-wall flaws

$$l_{crit} = 1.58(Rt)^{1/2}\{(\sigma_f/\sigma_h)^2 - 1\}^{1/2} \quad (1)$$

In Fig. 2, the ratio of flaw depth to wall thickness (a/t) shall be used to determine the appropriate failure assessment diagram curve. For the flaw depth range from 25 to 50 percent of the wall thickness ($0.25 < a/t < 0.50$), linear interpolation of the failure assessment diagram curves may be used.

The failure assessment diagram curves shown in Figs 1 and 2 shall have vertical cutoffs for upper bound limits on S_r. These cutoffs are discussed in reference **(16)**.

Failure assessment point coordinates denoted by (S'_r, K'_r) shall be calculated for the end of the evaluation period flaw dimensions and for stresses at the

location of, and normal to, the flaw using the J_R resistance curve data for elastic–plastic fracture where ductile flaw extension at upper shelf temperatures may occur prior to reaching limit load, or J_{IC} fracture toughness data at transition or lower shelf temperatures.

The equations necessary to calculate the failure assessment point coordinates (S'_r, K'_r) for part through wall circumferential flaws for ductile flaw extension, Δa, are given below. If the operating temperature is in the transition or lower shelf region, J_R should be replaced by J_{IC} and Δa set to zero.

$$S'_r = (\mathrm{SF})P_m/P'_m \tag{2}$$

where SF is given in Table 1 and P'_m is recalculated for each value of Δa. If the primary membrane stress P_m is not zero

$$P'_m = \sigma_y \gamma \Gamma_m \tag{3}$$

$$\gamma = -\frac{\pi}{8}\frac{P_b}{P_m} + \left\{\left(\frac{\pi}{8}\frac{P_b}{P_m}\right)^2 + 1\right\}^{0.5} \tag{4}$$

$$\Gamma_m = \frac{[R_2^2 - R_c^2 + \{1 - (\theta/\pi)\}(R_c^2 - R_1^2)]}{(R_2^2 - R_1^2)} \tag{5}$$

$$R_c = R_1 + a + \Delta a \tag{6}$$

If the primary membrane stress P_m is zero, then

$$S'_r = \frac{\pi P_b(\mathrm{SF})}{4\sigma_y \Gamma_m} \tag{7}$$

where Γ_m is recalculated for each value of Δa.

The coordinate K'_r is given by

$$K'_r = \sqrt{[J_e/J_R(\Delta a)]} \text{ for any value of } P_m \tag{8}$$

where J_e and J_R are also recalculated for each value of Δa.

The elastic J integral is given by

$$J_e = 1000\ K_I^2/E' \tag{9}$$

where

$$K_I = (\mathrm{SF})P_m\sqrt{(\pi a')}F_m + \{(\mathrm{SF})P_b + P_e\}\sqrt{(\pi a')}F_b \tag{10}$$

$$F_m = 1.1 + (a'/t)\left\{0.15241 + 16.722\left(\frac{a'}{t}\frac{\theta}{\pi}\right)^{0.855} - 14.944\left(\frac{a'}{t}\frac{\theta}{\pi}\right)\right\} \tag{11}$$

$$F_b = 1.1 + (a'/t)\left\{-0.09967 + 5.0057\left(\frac{a'}{t}\frac{\theta}{\pi}\right)^{0.565} - 2.8329\left(\frac{a'}{t}\frac{\theta}{\pi}\right)\right\} \tag{12}$$

$$a' = a + \Delta a \tag{13}$$

In the above equations, a' is updated after each increment of ductile flaw extension, while θ is fixed at its end of evaluation period value.

The equations necessary to calculate the failure assessment point coordinates (S'_r, K'_r) for axial flaws for ductile flaw extension, Δa, are given below. If the operating temperature is in the transition or lower shelf region, J_R should be replaced by J_{IC} and Δa set to zero

$$S'_r = (\mathrm{SF})p/P_0 \tag{14}$$

where SF is given in Table 1, and P_0 is recalculated for each value of Δa from

$$P_0 = \frac{2}{\sqrt{3}}\frac{(t - a^*)}{(R_1 + a^*)}\sigma_y \tag{15}$$

$$a^* = \frac{a'[1 - \{1 + 0.5(a'/t)^2/(a/l)^2\}^{-1/2}]}{[1 - (a'/t)\{1 + 0.5(a'/t)^2/(a/l)^2\}^{-1/2}} \tag{16}$$

The coordinate K'_r is given by equation (8), where

$$K_I = (\mathrm{SF})p(R_1/t)\sqrt{(\pi a'/Q)}F_1 \tag{17}$$

$$Q = 1 + 4.593(a/l)^{1.65} \tag{18}$$

$$F_1 = 0.97\{M'_1 + M'_2(a'/t)^2 + M'_3(a'/t)^4\}f_c \tag{19}$$

$$f_c = \{(R_2^2 + R_1^2)/(R_2^2 - R_1^2) + 1 - 0.5\sqrt{(a'/t)}\}t/R_1 \tag{20}$$

$$M'_1 = 1.13 - 0.18(a/l) \tag{21}$$

$$M'_2 = -0.54 + 0.445/(0.1 + a/l) \tag{22}$$

$$M'_3 = 0.5 - \frac{1}{(0.65 + 2a/l)} + 14(1 - 2a/l)^{24} \tag{23}$$

In the equations above, a' is updated after each increment of ductile flaw extension, while a/l is fixed at its end of evaluation period value.

The failure assessment point coordinates (S'_r, K'_r) are calculated for each loading condition using the safety factors (SF) given in Table 1 to determine flaw acceptance.

(a) For lower shelf and transition temperatures, Δa is set to zero and J_R is set to the J_{IC} at the temperature of interest in the calculation of the failure assessment point coordinate. Plot the assessment point on the appropriate failure assessment diagram. The assessment point must be inside the failure assessment curve to have the flawed pipe accepted for continued service.

(b) For upper shelf temperatures where ductile flaw extension may occur prior to reaching limit load, a series of assessment points for various amounts of ductile flaw extension, Δa, obtained from the J_R resistance curve shall be calculated and plotted on the appropriate failure assessment diagram. One or more of the calculated assessment points must be inside the failure assessment curve to have the flawed pipe accepted for continued service.

(c) In addition to satisfying (a) and (b), the S'_r coordinate of the assessment point must also satisfy

$$S'_r \leqslant S_r^{\text{cutoff}}$$

where S_r^{cutoff} is the limit load cutoff on the diagram assessment diagram.

Simplification of DPFAD for part-through-wall flaws

The deformation plasticity failure assessment diagram (DPFAD) procedure utilises deformation plasticity solutions **(6)(7)** for cracked structures in the format of the British Central Electricity Generating Board's (CEGB) R-6 two-criteria failure assessment diagram (FAD) **(8)** to graphically solve elastic–plastic fracture mechanics problems through the solution of the non-linear equation $J_{\text{applied}} = J_{\text{material}}$ for the load corresponding to the current crack length and tearing resistance. Since DPFAD was developed from the CEGB two-criteria R-6 approach, it not only handles elastic–plastic fracture but linear elastic fracture and net section plastic collapse or limit load of the flawed structure. DPFAD, however, is more accurate than the R-6 procedure for some geometries since the DPFAD curve accounts for changes in flaw depth versus component thickness while the R-6 curve reflects independence of the flaw depth to component thickness ratio. The general DPFAD procedure involves three steps.

(1) The generation of the DPFAD curve from elastic plastic analysis of a flawed structure using deformation plasticity solutions for a simple power-law strain-hardening material based on the Ramberg–Osgood stress–strain equation

$$\varepsilon/\varepsilon_0 = \sigma/\sigma_0 + \alpha(\sigma/\sigma_0)^n \tag{24}$$

where $\sigma_0 = \sigma_{ys}$ and $\varepsilon_0 = \sigma_{ys}/E$

If the J integral response of the structure can be represented by

$$J_{\text{applied}} = J_I^e + J_P \tag{25}$$

then

$$\frac{J_{\text{applied}}}{G} = \frac{1}{K_r^2} = (J_I^e + J_p)/G \tag{26}$$

or

$$K_r = \sqrt{(G/J_{\text{applied}})} = f(S_r) \tag{27}$$

where S_r is the ratio of applied stress to net section plastic collapse stress and

$$G = K_I^2/E' \tag{28}$$

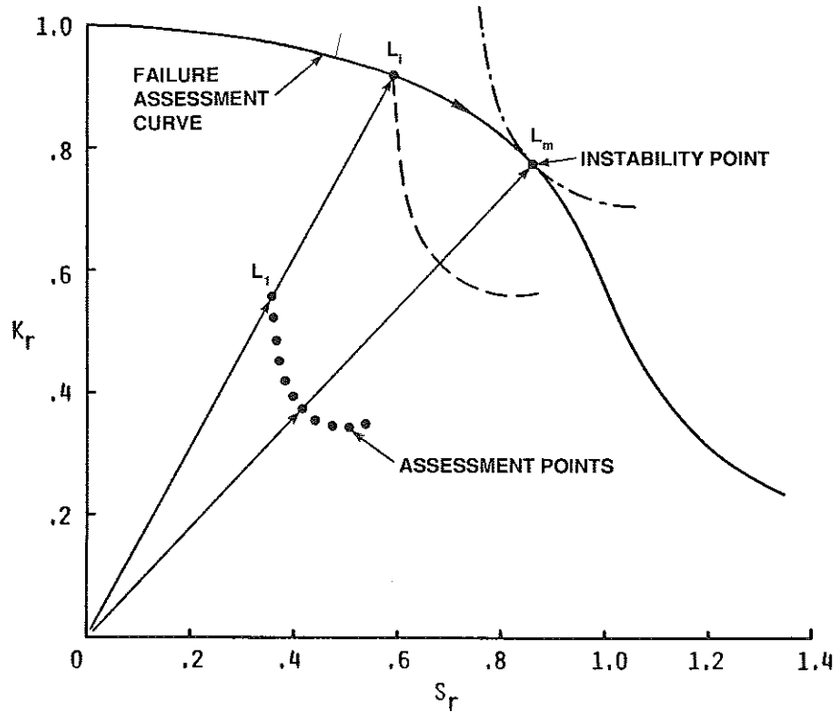

Fig 4 Illustration of instability point determination

The difference between J_I^e and G is that J_I^e includes the small-scale, yielding plastic zone correction while G does not. The resulting expression **(27)** defines a curve in the K_r-S_r plane that is a function of flaw geometry, structural configuration, and stress–strain behaviour of the material defined uniquely by α, n from equation (24). Because both K_r, S_r are linear in applied stress, the DPFAD curve is independent of the magnitude of applied loading.

(2) The determination of assessment points is based on the ratio of K_I or J_I (square root) of the structure divided by the relevant material property K_{IC} or J_{IC} (square root) at flaw initiation or for stable flaw growth, $J_R(\Delta a)$ (square root), the tearing resistance of the material for the ordinate, K'_r, and the ratio of the applied stress (load) to net section plastic collapse (limit load) for the abscissa, S'_r. For flaw initiation, a single assessment point is calculated. For stable crack growth, a locus of assessment points are determined by incrementing the crack size 'a' by '$a + \Delta a$' in the calculation of J_I for a constant applied load. The resulting locus is illustrated in Fig. 4 in the shape of a 'candy cane.'

(3) Crack initiation or tearing instability can be determined graphically by plotting the calculated assessment point(s) on the failure assessment diagram. For crack initiation, the single assessment point must fall on the DPFAD curve or outside the curve. For tearing instability, the critical instability load is determined by the tangency of the assessment locus with the DPFAD curve, as shown in Fig. 4. Any assessment point on a line from the origin of the diagram is directly proportional to load with any other point on that same line, and only one load level is needed to determine the instability load. The instability load is obtained by multiplying the applied load by the ratio of the distance from the origin to the point of intersection of the line with the DPFAD curve to the distance from the origin of the diagram to the applied load point.

The goal for simplification of the DPFAD methodology for part-through wall flaws in ferritic piping is to be able to handle all materials, flaw sizes, and pipe sizes with a minimum of DPFAD curves. The determination of the assessment points requires only the stress intensity factor and limit load expressions for the various flaw configurations, loading states, and pipe sizes. Formulations for J_I for circumferential through-wall and part-through wall flaws in cylinders under tension, bending, and combined bending and tension from reference **(9)** were used to generate DPFAD curves using PCFAD **(10)** for various combinations of α, n.

The initial comparisons of DPFAD curves were thought to require separate curves for each category of materials. Table 2 lists the tensile properties for ferritic piping materials required to compare the various DPFAD curves per α, n. The values of yield and ultimate strength were obtained from a study in **(11)**. The values of α, n were determined using equations from **(12)** knowing only σ_{ys}, σ_{uts}, and E. Figure 5 shows a comparison of DPFAD curves for the four categories of materials given in Table 2 for an axisymmetric crack under tension for a flaw depth of 50 percent of the wall thickness for a radius to thickness ratio of 10. From this figure it can be concluded that ferritic piping could be categorised according to only *three* groups of materials:

- base metal and 70XX SMAW welds;
- SAW welds;
- 80XX SMAW welds.

Table 2 Tensile properties for DPFAD for ferritic piping materials at 450–550°F

Material	*Condition*	*YS (ksi)*	*UTS (ksi)*	α*	n*	*DPFAD cutoff*
Base metal	—	31	65	2.64	4.42	2.10
70XX SMAW	PWHT	34	61	2.48	5.25	1.79
80XX SMAW	PWHT	73	88	1.62	10.78	1.21
SAW	PWHT	50	72	1.98	7.14	1.44
	$E = 26 \times 10^3$ (ksi)					

* Bloom's equation (EPRI NP-2431)

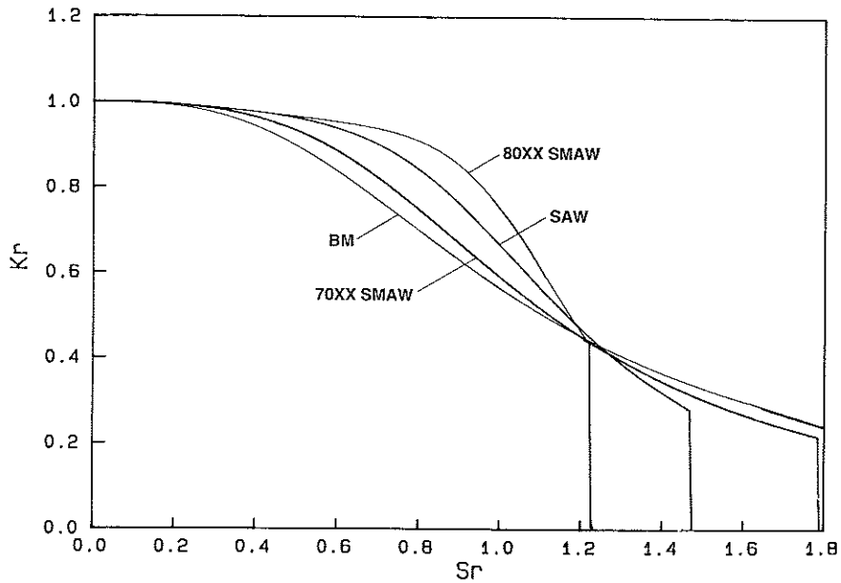

Fig 5 Comparison of ferritic material categories for axisymmetric flaw for $a/t = 0.5$ and $R/t = 10$

However, work shows that a flawed pipe with a weld can be evaluated using the stress–strain properties of the base metal and the toughness properties of the weldment **(13)**. Therefore, the DPFAD curve for ferritic piping could be represented by curves for the various flawed geometries of the pipe and the stress–strain properties of the base metal.

The pipe geometry, loading and crack depth to wall thickness effects were investigated next. Figure 6 demonstrates that the radius to thickness (R/t) effect is not significant. Figure 7 illustrates the effect of tension versus bending for a through-wall flaw in a cylinder with $R/t = 10$. Once part-through-wall flaw J solutions were available **(9)**, the effect of crack angle was investigated for $a/t = 0.5$, 0.75 for both bending and axial loadings. Figure 8 illustrates the effect of crack angle for $a/t = 0.5$ for axial loading. Figure 9 illustrates the same but for $a/t = 0.75$ and Fig. 10 illustrates the effect of bending versus axial loading through comparison with the lower bound curve of Fig. 9. Note that in both Figs 8 and 9 that the $2\theta = 27.5$ degrees, 45 degrees, 90 degrees, and 180 degrees DPFAD curves all fall close to one another, with the $2\theta = 90$ degrees forming a lower bound. Figure 10 and Fig. 8 show (as also demonstrated earlier in Fig. 7) that the DPFAD curves are independent of the loading condition, with the axial loading curve being slightly lower. Therefore, for part-through-wall circumferential flaws in ferritic piping, one DPFAD curve with lower bound stress–strain curve base metal properties for a geometry of $a/t = 0.5$, $R/t = 10$ and $2\theta = 90$ degrees under axial loading can

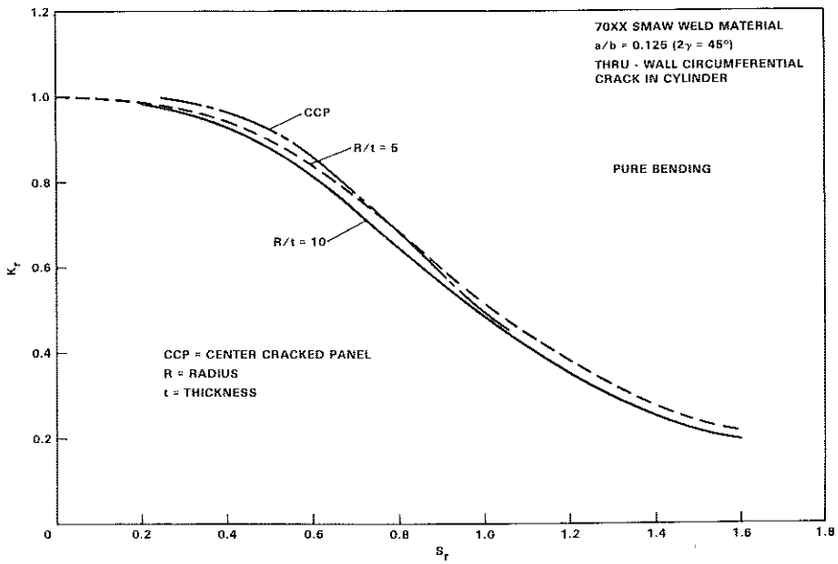

Fig 6 Comparison of R/t effects on DPFAD curves for through-wall circumferential flaw under pure bending

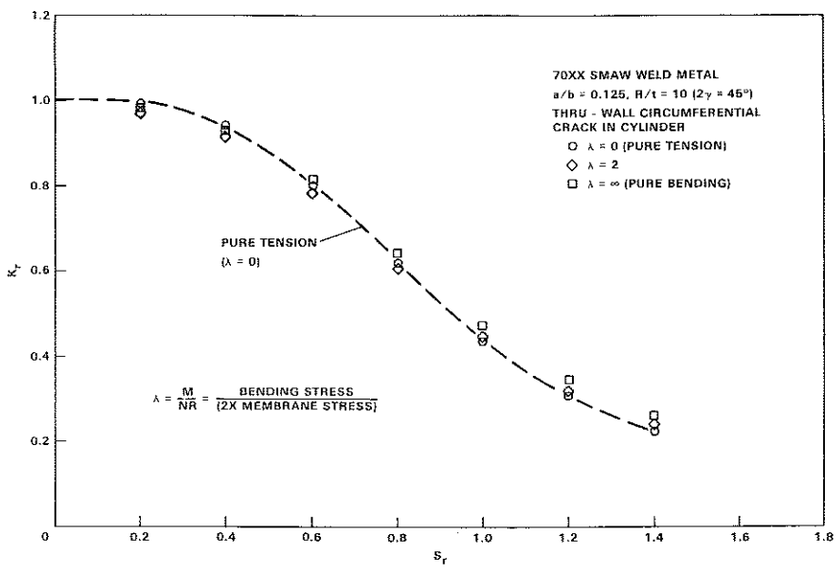

Fig 7 Comparison of effects of loading (bending versus tension) for through-wall circumferential flaw for 70XX SMAW weld metal

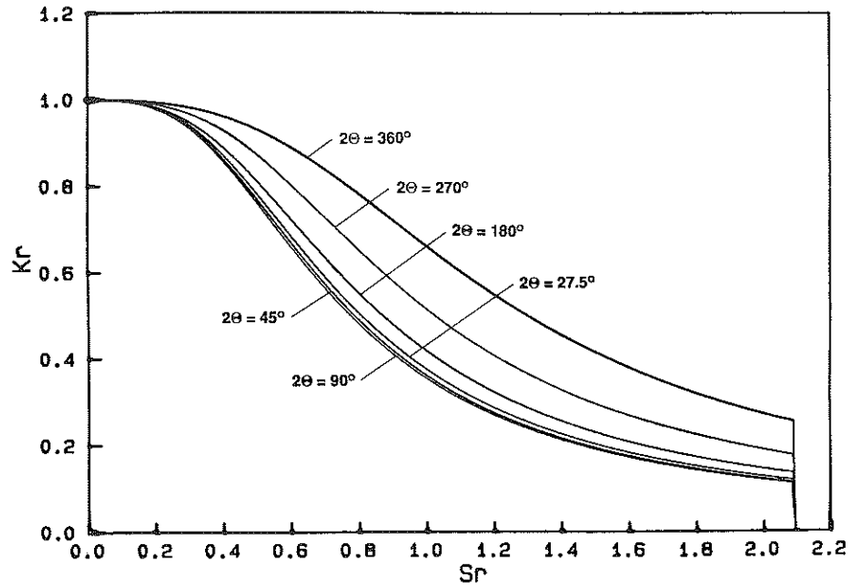

Fig 8 Comparison of θ variation for part-through-wall flaw in pipe under tensile loading with $a/t = 0.5$ for ferritic base metal

be used to represent all flawed ferritic pipes, providing the correct stress intensity factor and limit load expressions are used in the calculation of the assessment points, K_r', S_r' along with the appropriate toughness for the flawed region (weld or base metal) in terms of J_{IC} or $J_R(\Delta a)$. The resulting DPFAD curve for part-through-wall circumferential flaws in a ferritic pipe for $2\theta \leqslant 180$ degrees is shown in Fig. 1.

For part-through-wall axial flaws in ferritic piping under pressure loading, similar comparisons have been made to illustrate the effects of flaw depth to wall thickness and aspect ratio (flaw depth to flaw length). While aspect ratio and pipe size have been shown to be insigificant **(14)(15)**, flaw depth to wall thickness must be accounted for in the DPFAD curves. Two DPFAD curves shown in Fig. 2 for lower bound ferritic base metal for part-through-wall axial flaws in pipes under pressure loading are needed in the assessment of defects using the DPFAD approach.

The vertical cutoff of the DPFAD curves were originally set by

$$S_r^{\text{cutoff}} = \sigma_{\text{uts}}/\sigma_{\text{ys}} \tag{29}$$

This was demonstrated in reference **(12)**, where a modified Ramberg–Osgood curve accounting for ultimate or saturation stress was used to generate a DPFAD curve for an infinite centre-cracked plate. Since S_r' is defined here using the yield strength of the material, the actual material in the DPFAD

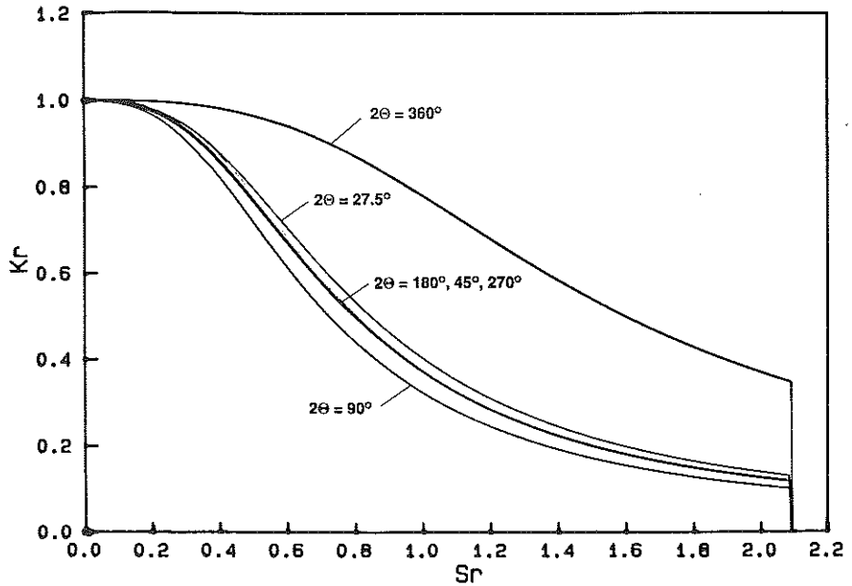

Fig 9 Comparison of θ variation for part-through-wall flaw in pipe under tensile loading with $a/t = 0.75$ for ferritic base material

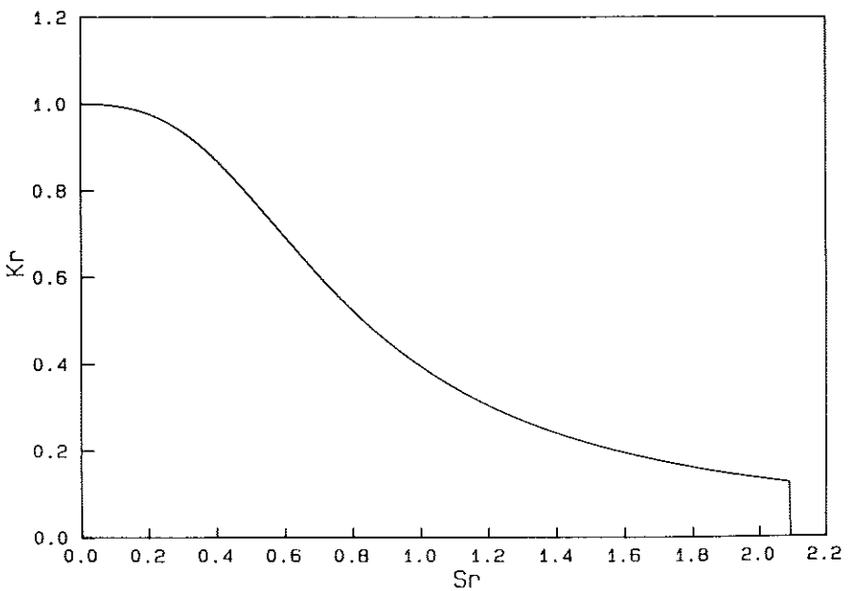

Fig 10 DPFAD curve for part-through-wall flaw $2\theta = 90$ degrees for pipe under bending with $a/t = 0.5$ for ferritic base metal

plane would saturate out at approximately

$$S_r^{cutoff} = P/P_{ultimate} \times \sigma_{uts}/\sigma_{ys} = \frac{\sigma_{uts}}{\sigma_{ys}} \quad (30)$$

However, to make this cutoff consistent with the limit load expressions given in Appendix Z **(3)** of code case N-463, limit load failure is assumed to occur at a critical flow stress, σ_f, which is defined as the average of σ_{ys} and σ_{uts}. Using this as well as the limit load expressions in Appendix Z will modify the vertical cutoffs in the general DPFAD approach. Further discussion can be found in reference **(16)**.

Validation of simplified approach

The validation of the simplified DPFAD approach for ferritic piping was accomplished through comparison of predicted failure loads using the DPFAD single curve for circumferential flaws and multiple curves (two) for axial flaws to the actual experimental failure loads for three sets of pipe experiments. The Battelle Columbus Laboratories (BCL) degraded piping program (Phase II) tests results from reference **(17)** are summarised in Table 3 for part-through-wall flawed ferritic pipes under pure bending ($P_m = 0$) as well as experiment 4131-4 under combined tension plus bending where internal pressure was held constant, producing $P_m = 10.2$ ksi. Table 4 summarises the JAERI test results **(18)** for Japanese tests of ferritic piping under pure bending. Lastly, Eiber/BCL **(19)** axial flawed pipe burst tests under pressure are summarised in Table 5. Plots produced using the Babcock & Wilcox computer code PCFAD **(10)** for each test were based on the actual failure pressures as input. The radial distances from the origin of the diagram to the assessment points (candy canes) to the corresponding point of the failure assessment curve is a measure of the conservatism of the simplified DPFAD approach.

The instability stress is the point connected with the line (dash-dot in Fig. 11 for specimen BCL 4112-9) from the origin to the failure assessment curve. The

Table 3 BCL tests (CSC) predictions using actual material properties

Exp. number	*4112-5*	*4112-6*	*4112-7*	*4112-8*	*4112-9*	*4115-1*	*4131-8*	*4131-4*
J_R curve*	F1-ZP13-3LC	F30-ZP15-3LC	ZP14-3LC	F29-17	F-13-19	F-9-17	F-9-17	F-9-17
σ_y (ksi)	30.8	46.4	37.5	34.4	38	34.7	34.7	34.7
σ_u (ksi)	67.8	90.0	82.7	88.5	88.7	76.5	76.5	76.5
σ_u/σ_y**	2.20	1.94	2.21	2.57	2.33	2.21	2.21	2.21
P_{bexp} (ksi)	36.7	43.4	47.5	36.8	34.5	38.3	36.5	27.0 (10.2***)
P_{bcal} (ksi)	33.5	31.5	32.9	26.0	32.1	31.3	30.7	23.7 (9.0***)
P_{bexp}/P_{bcal}	1.10	1.38	1.45	1.41	1.07	1.22	1.19	1.14

* Refers to BCL specimen ID number, all JR curves from non-side-grooved specimens. J_M or J_M* used in analysis

** DPFAD cutoff based on ultimate strength divided by yield strength

*** Membrane stress

Table 4 JAERI tests (CSC)

Exp. number	*CS-11*	*CS-12*	*CS-13*	*CS-15*	*CS-16*
J_{IC}* (lb/in)	2016	2016	2016	2016	2016
σ_y (ksi)**	80.6	35.6	35.6	35.6	35.6
P_{bexp} (ksi)	80.3	66.2	51.4	69.8	58.6
P_{bcal} (ksi)	62.9	47.7	37.0	52.1	45.0
P_{bexp}/P_{bcal}	1.28	1.39	1.39	1.34	1.30

* All JAERI test predictions based on initiation J_{IC} toughness
** DPFAD cutoff based on $s_u = 65$ KSI and s_u/s_y value

Table 5 EIBER/BCL axial flawed pipe burst tests

Exp. number	*AEC-8*	*AEC-18*	*AEC-19*	*AEC-20*
*Material**	*A106B*	*A106B*	*A106B*	*A106B*
Yield strength (ksi)	31.6	34.8	33.6	37.6
a/t	0.738	0.507	0.649	0.513
a/l	0.0518	0.0346	0.0905	0.0667
Test temp. (°F)	696	469	628	504
Test pressure at failure (psig)	2300	1620	4300	1960
Pressure at instability DPFAD (psig)	3147	1744	3812	1944
P_{exp}/P_{cal}	0.73	0.93	1.13	1.01

* Material toughness taken from pipe tests for CL orientation at 550°F representative of material with toughness of $J_{IC} = 277$ lb/in; J_R curve used from MEA specimen ZP13-1CL (lowest J_R curve)

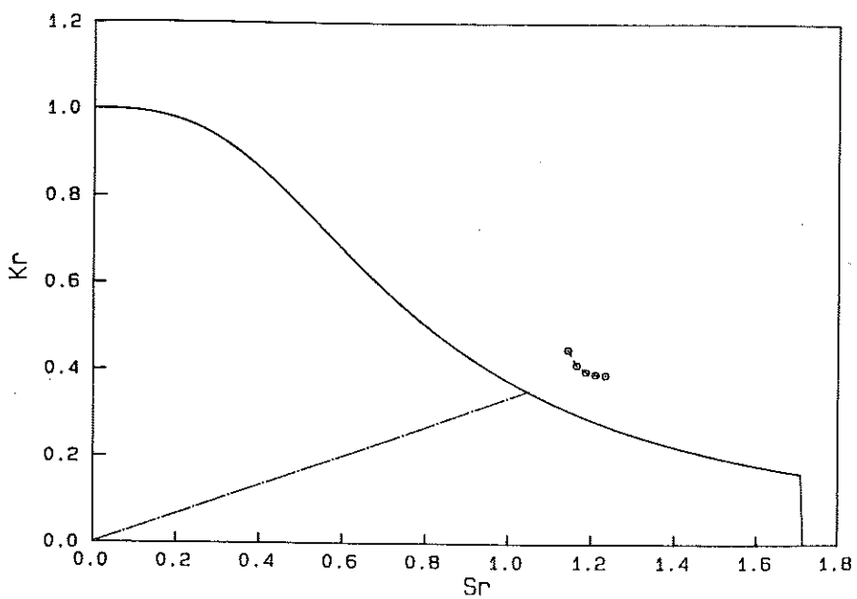

Fig 11 Failure loading locus per J_R resistance curve plotted in DPFAD space for BCL pipe test 4112–9

appropriate ratios along these lines give the P_{bexp}/P_{bcal} ratios in the tables. Table 3 presents the BCL (CSC) test predictions using actual BCL **(20)** compact test data (nonside grooved J_M^* resistance curves). The J_m^* is defined by BCL as the recommended ASTM E-24 J_R curve test procedure, where J is separated into elastic and plastic components. It was noted that there was little difference between J_M^* and J_M for the ranges of the J_R curves used in the predictions. In addition to using the actual material J_R curves, the actual yield and ultimate strengths were used for calculating pipe-specific 'α' and 'n' values in the generation of the DPFAD curves using PCFAD. The pipe-specific DPFAD curves are only slightly different from the lower-bound generic ferritic base metal curve using $\alpha = 2.51$ and $n = 4.2$. The effect of using the nongeneric α, n values is approximately +1 percent, while the degree of conservatism in the predictions varies from +45 to +7 percent.

Note that the DPFAD approach should always be somewhat conservative, since the DPFAD curve reflects the initiation flaw size. For ductile tearing, the curves would move outward from the origin a slight amount depending on how much ductile tearing occurs before instability. Further discussion can be found in reference **(5)**. In Table 4, the JAERI tests were predicted using J_{IC}, since no resistance curves were available. Note the consistency of the predictions in Table 4 for P_{bexp}/P_{bcal} from 1.28 to 1.39. Use of actual resistance curves would clearly bring these ratios closer to 1.0 (less conservative). The four axial flawed pipes under pressure in Table 5 were predicted using pipe material 'representative' of CL-oriented material with toughness of $J_{IC} =$ 277 lb/in. The J_R curve used was the lower bound of all piping material (A106B) tested by Material Engineering Associates (MEA) taken from reference **(3)**. Actual toughness measurements were not determined by BCL at the time of the AEC-designated pipe tests. The only measure of toughness reported was Charpy energy values of from 50 to 60 ft-lbs at the test temperatures.

The failure assessment point equations had to be adjusted to account for the external axial flaws of the AEC pipe tests. With the adjustment in the K_I and limit load equations, DPFAD-predicted failure pressures due to ductile crack growth were from 28 percent nonconservative for pipe AEC-8 to 12 percent conservative for pipe AEC-19, with an average prediction of 1 percent nonconservative. Figure 12 presents the DPFAD plot for specimen AEC-20, where the predicted failure pressure was within 1 percent of the experimental burst pressure. For test specimen AEC-8, the prediction was 28 percent nonconservative. On examination of Fig. 13 for the AEC-8 pipe, it is observed that the failure mode is close to ultimate strength limit load (the intersection of the dash-dot line with the vertical line, $S_r = 2.34$). If the limit load is defined by the flow stress equal to the average of yield and ultimate strengths, the new cutoff would be at $S_r = 1.58$, and the predicted failure pressure would be significantly reduced and near the actual failure pressure given in Table 5. Two additional pipe experiments, AEC-4 and AEC-9 (not reported in Table 5), displayed similar limit load behaviour at failure when plotted in DPFAD space. Addi-

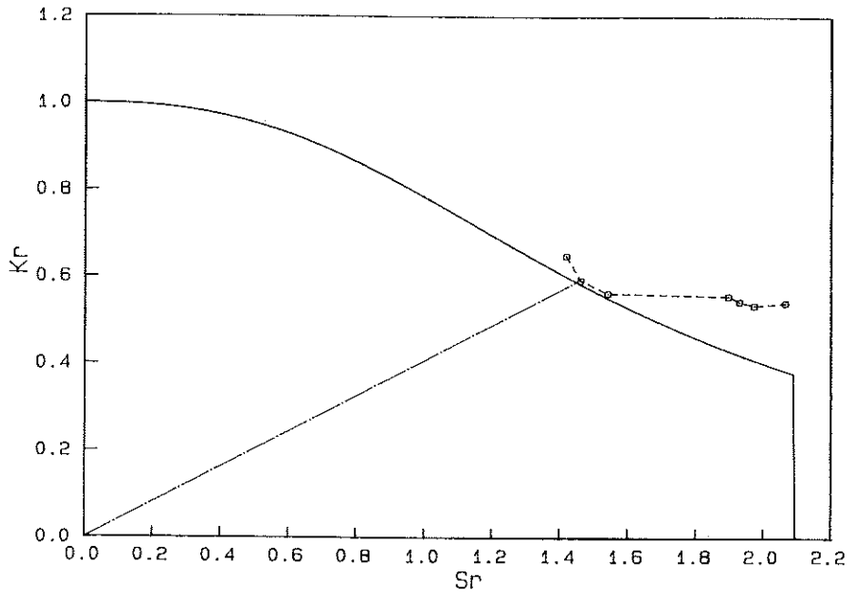

Fig 12 Failure pressure locus for J_R resistance curve plotted in DPFAD space for AEC 20 pipe test

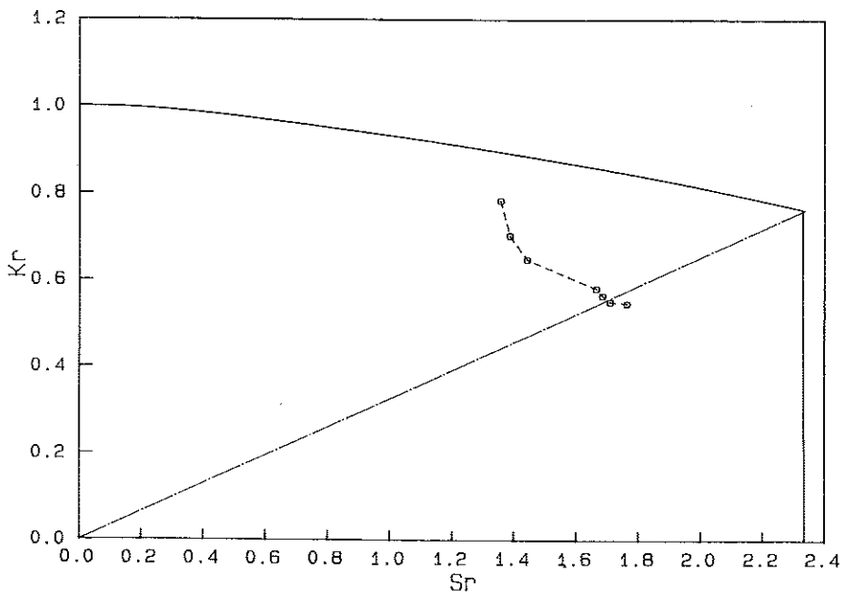

Fig 13 Failure pressure locus per J_R resistance curve plotted in DPFAD space for AEC 8 pipe test

tional details of the axial flawed pipe experiments can be found in reference **(15)**.

Conclusions

A simple procedure for evaluating the acceptability of flaws detected in ferritic piping using the DPFAD methodology has been presented. It has been shown that the general DPFAD approach for flawed ferritic piping can be reduced to one DPFAD curve for the assessment of part-through-wall circumferential flaws and two DPFAD curves for the assessment of part-through-wall axial flaws. Validation of the simplified approach has been demonstrated through comparisons with actual experimental test results of degraded nuclear piping.

References

(1) *ASME Boiler and Pressure Vessel Code* (1989) ASME, New York (and Addenda).
(2) 10 CFR (1984) *Code of Federal Regulations Part 50*, United States Government.
(3) Evaluation of flaws in ferritic piping (1988) Electric Power Research Institute Final Report NP-6045, Palo Alto, CA.
(4) BLOOM, J. M. (1983) Validation of a deformation plasticity failure assessment diagram approach to flaw evaluation, *Elastic–Plastic Fracture: Second Symposium* **II** – *Fracture Resistance Curves and Engining Appl, ASTM STP 803*, (Edited by C. F. Shih and J. P. Gudas), ASTM, Philadelphia, pp. II-20-6–II-238.
(5) BLOOM, J. M. (1985) Deformation plasticity failure assessment diagram, *Elastic–Plastic Frac Mech Technology, ASTM STP 896*, (Edited by J. C. Newman, Jr. and E. F. Loss), ASTM, Philadelphia.
(6) KUMAR, V., GERMAN, M. D., and SHIH, C. F. (1981) An engineering approach for elastic–plastic fracture analysis, Topical Report No. EPRI NP-1931, Research Project 1237-1, General Electric, Schenectady, NY.
(7) KUMAR, V., GERMAN, M. D., WILKENING, W. W., ANDREWS, W. R., deLORENZI, H. D., and MOWBRAY, D. F. (1984) Advances in elastic–plastic fracture analysis, EPRI Final Report No. NP-3607, Research Project 1237-1, General Electric Company, Schenectady, NY.
(8) MILNE, I., AINSWORTH, R. A., DOWLING, A. R., and STEWART, A. T. (1986) Assessment of the integrity of structures containing defects, Central Electricity Generating Board, Report R/H/R6-Rev. 3.
(9) KUMAR, V. and GERMAN, M. D. (1988) Elastic–plastic fracture analysis of through-wall and surface flaws in cylinders, EPRI Final Report NP-5596, Research Project 1237-5, General Electric Company, Schenectady, NY.
(10) BLOOM, J. M. (1987) User's Guide for the Failure Assessment Diagram – Computer Code 'FAD', Babcock & Wilcox Report, Babcock & Wilcox Alliance Research Center, Revision 3a.
(11) ZAHOOR, A., GAMBLE, R. M., MEHTA, H. S., YUKAWA, S., and RANGANATH, S. (1986) Evaluation of flaws in carbon steel piping, EPRI NP-4824M and NP-4824SP.
(12) BLOOM, J. M. and MALIK, S. N. (1982) A procedure for the assessment of the integrity of nuclear pressure vessels and piping containing defects, EPRI Topical Report NP-2431, Research Project 1237-2, Electric Power Research Institute, Palo, Alto, CA.
(13) GANTA, B. R., AYRES, D. J., and NORRIS, D. M. (1987) Analysis of a pipe weldment with a circumferential through-wall crack, ASME PVP paper 87-PVP-34, presented at the Pressure Vessel and Piping Conference, San Diego, CA.
(14) BLOOM, J. M. (1986) Extensions of the failure assessment diagram approach semi-elliptical flaw in pressurized cylinders – Part II, *J. Pressure Vessel Technol.*, **108**, 485.
(15) BLOOM, J. M. (1990) Validation of the deformation plasticity failure assessment diagram (DPFAD) approach – the case of an axial flaw in a pressurized cylinder, *J. Pressure Vessels Piping*, **112**.

(16) EPRI (1990) Technical support document for Appendix J – DPFAD approach for the evaluation of flaws in ferritic piping, *Electric Power Research Institute, EPRI* Research Project 1757-34, to be published.
(17) WILKOWSKI, G. M. *et al.* (1984–5) Degraded piping program phase II, Semi-annual Report, NUREG/CR-4082, BMI-2120, **2**.
(18) NORRIS, D. M. and KISHIDA, K. (1987) Evaluation of flaws in nuclear piping, presented at the SMIRT Conf. held at Lausanne, Switzerland, Paper Number GF5/1.
(19) EIBER, R. *et al.* (1971) Investigations of the initiation and extent of ductile pipe rupture, BMI-1980, Columbus, OH.
(20) MARSHALL, C. W. (1987) Mechanical property data for samples machined from six different carbon steel pipes, private communication.